Acta Chemica Scandinavica A 38 (1984) 625–639

The Structures of Zinc Bromide Complexes in Aqueous Solution

PETER L. GOGGIN,[a] GEORG JOHANSSON,[b] MASUNOBU MAEDA,[b,*] and HISANOBU WAKITA[b,**]

[a] Department of Inorganic Chemistry, The University, Bristol BS8 1TS, England and [b] Department of Inorganic Chemistry, Royal Institute of Technology, S-100 44 Stockholm, Sweden

The structures of complexes formed between zinc and bromide ions in aqueous solution have been determined from large-angle X-ray scattering measurements and Raman and IR spectra. In the hydrated Zn^{2+} ion the coordination is octahedral with $Zn-H_2O$ distances of 2.10(1) Å. The highest bromide complex formed, $ZnBr_4^{2-}$, is tetrahedral with a Zn–Br bond length of 2.405(4) Å. In the lower complexes, $ZnBr_3^-$ and $ZnBr_2$, the Zn–Br bond has decreased slightly to 2.38 Å. $ZnBr_3^-$ is pyramidal with the Br–Zn–Br angle 115° and about the same angle is found for the bent $ZnBr_2$ structure. Water molecules are probably coordinated to Zn in the $ZnBr_3^-$ and the $ZnBr_2$ complexes, resulting in approximately tetrahedral structures, but unambiguous evidence for this cannot be obtained with the methods used. For the same Br–Zn ratio complex formation is enhanced by increased Zn^{2+} concentration, reflecting the lower activity of water in the more concentrated solutions. None of the techniques used indicates the presence of Zn Br Zn bridging.

The halide complexes formed by Zn^{2+}, Cd^{2+} and Hg^{2+} have been extensively studied.[1] The stepwise formation of the complexes leads from a hydrated metal ion, presumably octahedrally coordinated, to a tetrahedral coordination in MX_4^{2-}, the highest complex formed.

Stability constants show that Zn^{2+}, the hardest acceptor in the group, forms the weakest complexes and that the ranges of existence of the species formed by stepwise addition overlap. Thermodynamic data, in particular variations in ΔS values, indicate that in aqueous solutions a change in coordination takes place at the second step, that is on the addition of the second halide ligand.[2] The structures of the intermediate complexes are not, however, known. Previous X-ray diffraction measurements,[3–7] which have been primarily concerned with the chlorides,[3–5] have been interpreted as being consistent with tetrahedral structures. Exafs measurements on nearly saturated $ZnBr_2$ solutions (~9.5 M),[8] using the K absorption edges of Zn and Br, have been interpreted to show a local order of corner sharing $ZnBr_4$ tetrahedra, resembling that found in crystals. Most of the Zn^{2+} ions should, according to these measurements, occur in such extended units rather than as discrete ZnX_4^{2-} complexes. Raman measurements[9–16] on aqueous chloride and bromide solutions are consistent with a tetrahedral structure for the ZnX_4^{2-} complex but are less unambiguous in regard to the structures of the lower complexes.

In the present work an attempt has been made to get more detailed information on the structures of the complexes by using X-ray and spectroscopic (Raman and IR) data. The bromides have been chosen rather than the chlorides as this should increase the possibility of identifying, from X-ray scattering data, ligand–ligand interactions within the complexes. Iodide solutions will be treated in a separate paper.

Contributions from intramolecular interactions to the scattering data are relatively small and in order to distinguish changes in these interactions, when Zn–Br ratios are changed, the compositions of the solutions were chosen so as to

* Present address: Nagoya Institute of Technology, Gokiso, Showa-ku, Nagoya, 466, Japan.

** Present address: Department of Chemistry, Faculty of Science, Fukuoka University, Fukuoka 814, Japan.

0302-4377/84 $2.50

minimize simultaneous changes in intermolecular interactions. In two series of solutions, A and B, the bromide concentration was kept constant at 15 M and 5 M, respectively, and the Br–Zn ratio was varied from two to five by replacing Zn^{2+} in a pure $ZnBr_2$ solution by Li^+. In a third series of solutions, C, the bromide ions in a 3 M $ZnBr_2$ solution were gradually replaced by perchlorate ions keeping the Zn^{2+} concentration constant. Raman data, collected for the same solutions, were used to estimate relative concentrations of the complexes.

EXPERIMENTAL

Preparations. Analytical grade $ZnBr_2$, LiBr and $Zn(ClO_4)_2(H_2O)_6$ were dissolved in distilled water to the concentrations needed. The compositions of the solutions are given in Table 1.

X-Ray scattering measurements. The X-Ray scattering from the free surface of the solution was measured with MoK radiation in a $\theta-\theta$ diffractometer, described in previous papers.[17] A focusing LiF single crystal monochromator was positioned between the sample and the scintillation counter. Measurements were made at discrete θ values at intervals of 0.1° for $1°<\theta<20°$ and 0.25° for $20°<\theta<70°$. Three different slit widths, 1/12, 1/4 and 1° were used to cover the complete θ range. For each point, 100 000 counts were taken and each solution was scanned twice, resulting in a standard deviation of 0.22 % in the number of counts for each point.

Raman data. Raman spectra were excited using 514.5 nm irradiation from a Coherent Radiation Laboratories Model 52 argon ion laser (800 mw at the sample). Scattered radiation was analyzed using a Coderg T800 triple monochromator with a 4 cm^{-1} spectral slit width, and detected using a cooled photomultiplier (E.M.I. 9558 A) coupled to a Brookdeal 5CI photon counter. The digitized output was interfaced to an Apple II microcomputer. For spectral processing data were transferred to a Nicolet 1180 computer programmed to accept Raman spectra into the file structure of the Nicolet $F\cdot t\cdot i\cdot r$ software system, which was used for interactive spectral subtraction (*e.g.* the low wavenumber profile of water). The interactive curve analysis program of the Nicolet system was also used for deconvolution of composite bands.

IR data. Infrared spectra were measured with a Nicolet 7199A Fourier transform system in the far IR (500–50 cm^{-1}) using a 6.25 μm Mylar beam splitter, Globar source and polyethylene-windowed DTGS detector. Samples were contained in sealed cells with silicon windows. Sample thicknesses were *ca.* 12 μm, accurately determined by measurements of interference fringes from the empty cell. Spectral manipulation (spectral subtraction etc.) was carried out using the standard software of the Nicolet system.

DATA TREATMENT

X-Ray data. The X-ray scattering data were handled by means of the KURVLR and PUTSLR programs.[18] The intensity data were corrected for absorption, polarization and multiple scattering to give $I_{obs}(s)$, where $s=(4\pi/\lambda)\times \sin\theta$. The reduced intensity data, $i(s)$, were then calculated as

Table 1. Compositions of solutions.

	A1	A2	A3	B1	B2	B3	C1	C2	C3
Zn^{2+} mol l^{-1}	7.57	5.19	2.98	2.51	1.64	1.00	3.01	3.01	3.02
Br^- mol l^{-1}	15.14	15.53	14.85	5.02	5.07	5.01	–	1.50	3.03
Li^+ mol l^{-1}	–	5.16	8.90	–	1.79	3.00	–	–	–
H_2O mol l^{-1}	33.9	31.6	32.9	49.5	48.4	48.0	67.1	62.4	57.2
ClO_4^- mol l^{-1}	–	–	–	–	–	–	6.03	4.52	3.00
V Å^3	109.7	106.8	111.8	331.1	327.5	331.8	551.0	552.1	550.4
Zn atoms/V	0.50	0.33	0.20	0.50	0.32	0.20	1	1	1
Br atoms/V	1	1	1	1	1	1	–	0.50	1
Li atoms/V	–	0.33	0.60	–	0.35	0.60	–	–	–
H_2O atoms/V	2.24	2.03	2.21	9.87	9.55	9.59	14.3	14.7	15.0
ClO_4^- atoms/V	–	–	–	–	–	–	2.00	1.50	0.99
Br–Zn ratio	2.00	3.00	4.99	2.00	3.09	5.00	0	0.50	1.01

$$i(s)=KI_{obs}(s)-\sum_i n_i\cdot\{f_i(s)^2+\mathrm{del}(s)\cdot I_i^{incoh}(s)\}$$

K is a normalization constant chosen to refer all intensities to a stoichiometric unit of volume containing one Br atom in solutions A and B and one Zn atom in solutions C (Table 1). The normalization was performed by comparing observed intensity values in the high-angle part of the intensity curve with the calculated sum of independent coherent and incoherent scattering or by the integration method of Norman[19] and Krogh-Moe.[20] No significant deviations between the two methods were found. Scattering factors, $f_i(s)$, for neutral atoms were used with corrections for anomalous dispersion.[21] Values for incoherent scattering[22,23] were corrected for the Breit-Dirac effect. The del(s) function gives the estimated amount of incoherent radiation passing through the monochromator. It was checked in the high-angle part of the intensity curves by comparing measurements with a Zr filter placed either before or after the sample. The summation is made over the "i" different atomic species in the stoichiometric unit of volume. Corrections were made for low-frequency variations in the reduced intensities, leading to spurious peaks in the $D(r)$ functions below about 1.2 Å, not attributable to interatomic distances.[18] Observed $s\cdot i(s)$ values are shown in Fig. 1.

Electronic radial distribution functions were calculated from

$$D(r)=4\pi r^2\rho_o+2r/\pi\int_0^{s_{max}} s\cdot i(s)\cdot M(s)\cdot\sin(rs)\,ds$$

where $\rho_o=(\Sigma n_i Z_i)^2/V$, with Z_i the atomic number of atom "i" and V the stoichiometric unit of volume. The modification function, $M(s)$, was given the value

$$M(s)=f_{Zn}^2(0)\cdot f_{Zn}^{-2}(s)\,\exp(-0.003\cdot s^2)$$

which was used for all calculations, although for at least some of the solutions the quality of the data would have allowed a stronger sharpening without introducing disturbing ripples in the distribution functions.

Theoretical intensities for discrete interactions were calculated from the Debye expression:

$$i(s)=\sum_p\sum_{p\neq q}\sum_q f_p f_q\,\sin(sr_{pq})/sr_{pq}\exp(-b_{pq}s^2)$$

where r_{pq} is the distance between the two atoms involved and b is related to the root mean square variation in the distance: $l_{pq}=(2b_{pq})^{1/2}$. Non-discrete intermolecular interactions were approximated by assuming the complexes to occupy spherical holes in a continuous electron distribution.[18] Fourier inversions of theoretical intensity curves were calculated in the same way as for the experimental data.[18]

Raman data. Relative integrated intensities of the symmetric stretching bands of $ZnBr_4^{2-}$, $ZnBr_3^-$, $ZnBr_2$ and $ZnBr^+$ have been determined by Macklin and Plane[15] as 0.97, 1.0, 0.47 and 0.22, respectively. The experimental data were first subjected to solvent subtraction to yield a flat base line over the Zn–Br stretching region. Using a Lorenzian curve form, the Zn–Br stretching bands were deconvoluted using the curve analysis program with baseline level, base-

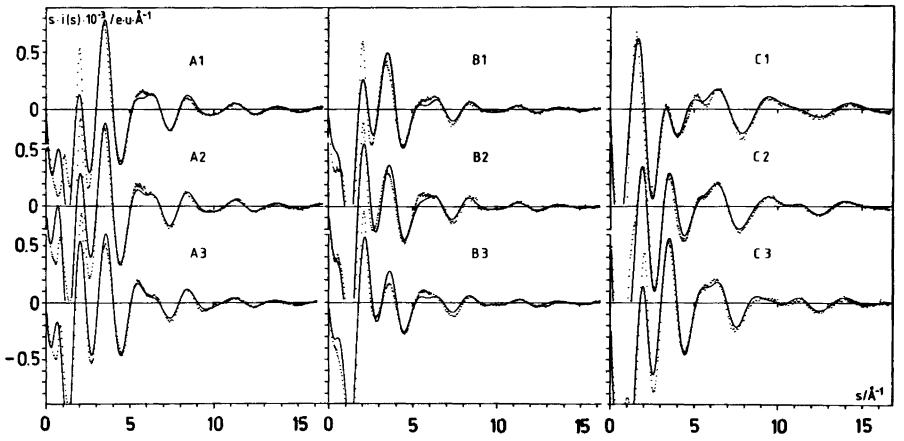

Fig. 1. Observed $s\cdot i(s)$ values (dots) compared with calculated values (solid lines) obtained with the use of parameters from Tables 2 and 5.

line slope and band height, width and position as variables. The program uses a simplex method to achieve a best fit, but it is usually possible to obtain a marginal reduction in the R.M.S. error between the experimental and synthesized curves by manual adjustment of the parameters, in interactive mode. Initially, each spectrum was analyzed independently, but this led to small differences in band parameters between spectra. The average of values for the band parameters were then preset and the analysis repeated. Comparison between the two sets of results indicates that the relative intensities of bands, which constitute more than one fifth of the total envelope, are accurate to ±5 %. The results are given in Table 6.

In this analysis, no allowance has been made for contribution from Zn–Br stretching vibrations other than the totally symmetric modes: comparison between the spectra of solution A3 under parallel and perpendicular polarisation conditions showed that the contribution from ν_3 to the total Zn–Br stretching band intensity of $ZnBr_4^{2-}$ was less than 2 %.

IR data. As measured, the spectra contain major contributions from the solvent and solvated cations. In order to examine features due to zinc bromide species more clearly, we have tried to eliminate most of the intensity from these factors by spectral subtraction. Because aqueous slutions of lithium salts show a greater absorbance above 400 cm^{-1} than does water itself, we have approached spectral subtraction in two steps. We have (a) a spectral file 4 mol dm^{-3} "$LiBr \cdot 4H_2O$" obtained by weighted subtraction of a water spectrum corresponding to residual water, and (b) the water spectrum. For subtraction from the zinc bromide solutions, we apportioned the water content as 4 molecules per Li, n molecules per $ZnBr_{4-n}(H_2O)_n$ on the basis of the Br–Zn ratio, and free water; (a) and (b) were subtracted accordingly (an example is shown later in Fig. 8; see also Ref. 24). This is admittedly rather arbitrary but does lead to spectra on a flatter base line across the Zn–Br stretching region which are subsequently used for interactive subtraction in attempts to isolate the spectra of individual species.

Some studies were also carried out using methanol as solvent and the solvent and cation effects were allowed for in a similar manner.

DISCUSSION OF THE STRUCTURES

Diffraction data. In the radial distribution curves (Fig. 2) peaks occur at expected intramolecular distances: Zn–H_2O at 2.0 Å, Zn–Br at 2.4 Å, Br–Br at 4.0 Å and, for the C solutions, Cl–O at 1.4 Å. The ratios between the Br–Br and the Zn–Br distances are close to $\sqrt{8/3}$= 1.63, the expected value for a tetrahedral arrangement. The intramolecular Zn–Br and Br–Br interactions are the dominant contributors to the outermost parts of the intensity curves (s>~3.5 $Å^{-1}$, see Fig. 3). Values for the parameters characterizing them, that is, distance (d), temperature coefficient (b), and frequency (n), could, therefore, be obtained by a least-squares refinement using the high-angle part of the intensity curves. The results, given in Table 2, show for the A3 solution that the number of Zn–Br interactions per Br atom is 0.80(2), corresponding to 5·0. 80=4.00(10) per Zn atom, that is the expected value if all Zn^{2+} ions occur as $ZnBr_4^{2-}$ complexes. The value of 1.630 for the ratio between the Br–Br and the Zn–Br distances does not differ significantly from $\sqrt{8/3}$=

Table 2. Results of least-squares refinement.[a]

	A1	A2	A3	B1	B2	B3
Zn—Br d Å	2.386(5)	2.398(4)	2.405(4)	2.365(5)	2.383(4)	2.385(4)
Zn—Br b Å²	0.004(1)	0.004(1)	0.003(1)	0.006(2)	0.003(1)	0.004(1)
$n_{Zn—Br}$/Br	1.02(5)	0.98(4)	0.80(2)	0.67(6)	0.65(5)	0.52(4)
$n_{Zn—Br}$/Zn	2.04(10)	2.93(12)	4.00(10)	1.34(12)	1.82(15)	2.25(20)
Br—Br d Å	3.98(1)	3.97(1)	3.92(1)	4.00(1)	3.95(2)	3.95(2)
Br—Br b Å²	0.036(5)	0.018(5)	0.029(10)	0.01(1)	0.03(1)	0.03(1)
$n_{Br—Br}$/Br	1.5(1)	1.1(1)	1.9(2)	0.5(1)	1.0(2)	0.7(1)
$d_{Br—Br}/d_{Zn—Br}$	1.668	1.656	1.630	1.691	1.658	1.656
av. Br—Zn—Br angle/°	113	112	109	115	112	112

[a] C1: $Zn(H_2O)_6$ d=2.10(1), b=0.012(2); ClO_4^- d_{Cl-O}=1.415(3), b_{Cl-O}=0.0008(2).

1.633 for a regular tetrahedron. Subtraction of the $ZnBr_4^{2-}$ contribution from the experimental distribution curve leaves a smooth background curve lacking features which can be related to the presence of polynuclear complexes (Fig. 4).

The occurrence of all Zn^{2+} as $ZnBr_4^{2-}$ units in the A3 solution is consistent with its Raman spectrum, which shows only one polarised peak at 171 cm^{-1}, the position of the symmetric stretching vibration, ν_1, for $ZnBr_4^{2-}$ (Fig. 8).

Replacement of Li^+ by Zn^{2+} leads to an increase of the Zn–Br frequency to one Zn–Br interaction per Br atom in the A2 and A1 solutions (Table 2). Thus, in these solutions, the

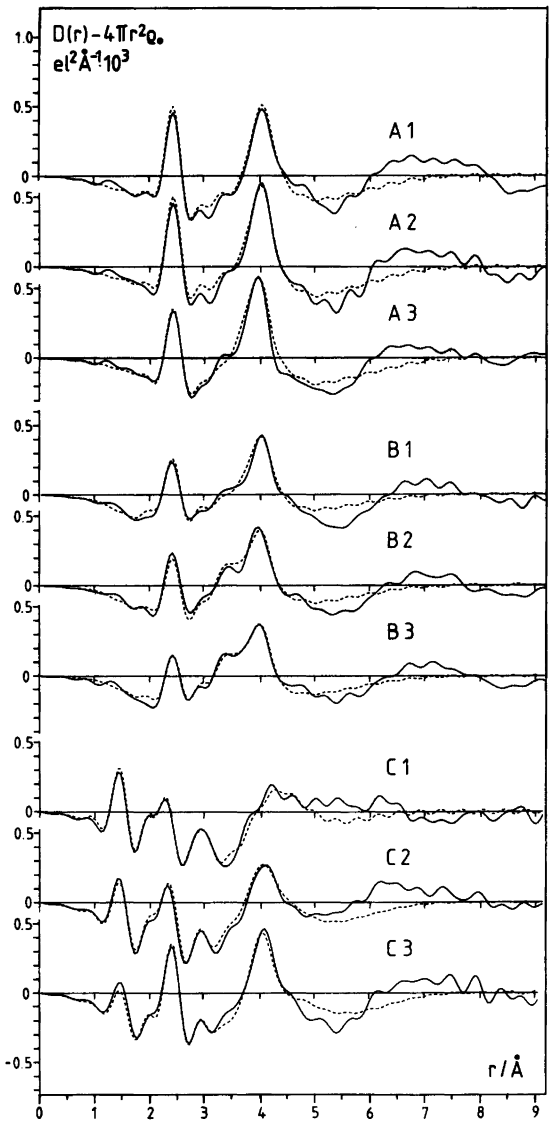

Fig. 2. Radial distribution functions, $D(r)-4\pi r^2\rho_0$, calculated from observed intensity values (solid lines) compared with theoretical curves (dashed lines) obtained with the use of parameters in Tables 2 and 5.

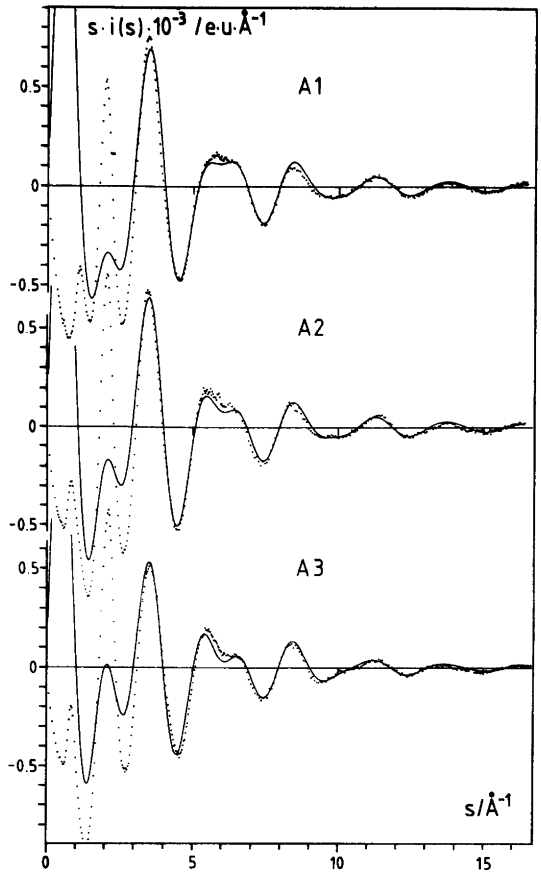

Fig. 3. Observed $s \cdot i(s)$ values (dots) for the A series of solutions (Table 1) compared with calculated values (solid lines) including only intramolecular interactions.

average Br atom forms only one Zn–Br bond and, since the Zn^{2+} concentration increases from A3 to A1, fewer Br atoms become bonded to each Zn. This is consistent with the Raman spectra, which for these solutions show the presence of three overlapping peaks at the positions of the symmetric polarised stretching vibrations corresponding to the three complexes $ZnBr_4^{2-}$, $ZnBr_3^-$ and $ZnBr_2$ (Figs. 8 and 9).

The relative concentrations of the complexes can be estimated from the Raman spectra by resolving the composite bands into their component peaks and using the relative intensity parameters derived by Macklin and Plane.[15] By combining the derived values with the Zn–Br frequencies, obtained in the least-squares refinements of the scattering curves, absolute concentrations for the complexes can be estimated (Table 3).

With decreasing Br–Zn ratios the least-squares refinements (Table 2) show a continuous decrease in the Zn–Br and an increase in the Br–Br distances, indicating a slight increase in the Br–Zn–Br angle within the complexes from the value of 109.5° in a tetrahedron. By using the parameter values determined for $ZnBr_4^{2-}$ (Table 2) and for the concentrations of the complexes (Table 3) the structural parameters for the lower complexes $ZnBr_3^-$ and $ZnBr_2$ were estimated both from new least-squares refinements, and from the values in Table 2 by assuming them to represent weighted averages of the different complexes. The results were the same for either method and are given in Table 4.

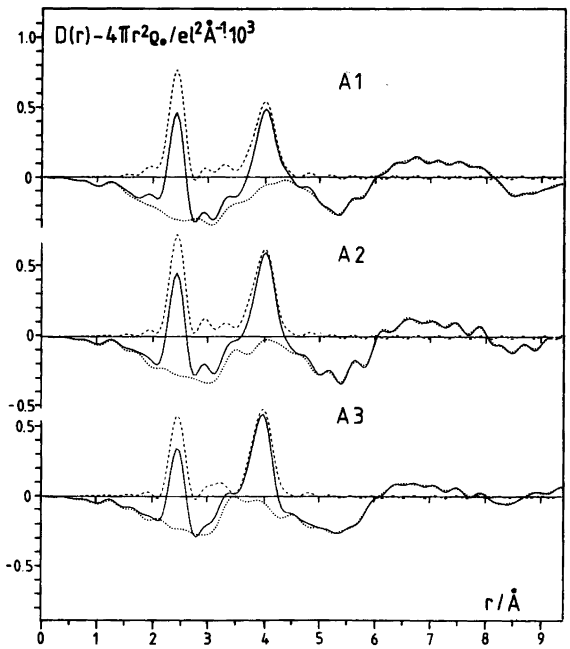

Fig. 4. Experimental $D(r)-4\pi r^2\rho_0$ functions (solid lines) for A solutions (Table 1) compared with values (dashed lines) calculated for intramolecular interactions only (Tables 2 and 5). The difference between the two curves is given by the dotted line.

The average Br–Zn–Br angle, obtained for the $ZnBr_3^-$ and $ZnBr_2$ complexes is ~115°. There is a slight increase in this angle, although not significant, with an increasing relative concentration of $ZnBr_2$.

We conclude that the $ZnBr_3^-$ complex is pyramidal with the Br–Zn–Br angle about 114°, that is between those in a tetrahedron (109.5°) and in

Table 3. Concentrations of complexes as estimated from Raman and X-ray data.

mol l^{-1}	A1	A2	A3	B1	B2	B3	C1	C2	C3
$ZnBr_4^{2-}$	1.17	1.88	2.98	0.36	0.45	0.44	–	0.06	0.19
$ZnBr_3^-$	2.28	2.00	–	0.48	0.41	0.25	–	0.22	0.43
$ZnBr_2$	1.98	0.87	–	0.25	0.13	0.04	–	0.27	0.45
$ZnBr^+$	–	–	–	–	–	–	–	0.07	0.07
Zn^{2+}	2.14	0.44	–	1.42	0.65	0.27	3.01	2.39	1.88
Br^-	–	0.27	2.93	1.64	1.78	2.42	–	–	–

Table 4. Structural parameters for the lower complexes $ZnBr_3^-$ and $ZnBr_2$.

	A1	A2	A3	B1	B2	B3
$[ZnBr_2]/[ZnBr_3^-]$	0.9	0.4	–	0.5	0.3	0.2
d_{Zn-Br} Å	2.386	2.390	–	2.365	2.366	2.360
d_{Br-Br} Å	4.01	4.00	–	4.04	3.98	3.99
Λ Br—Zn—Br°	115.2	113.6		117.3	114.5	115.4

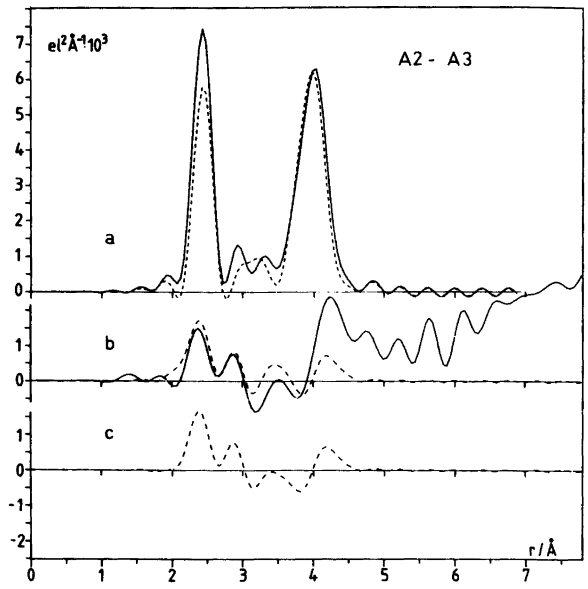

Fig. 5. a. Peak shapes calculated for complexes in the A2 (solid line) and the A3 solution (dashed line) including $ZnBr_4^{2-}$, $ZnBr_3H_2O^-$, $ZnBr_2(H_2O)_2$, $Zn(H_2O)_6^{2+}$ and $Li(H_2O)_6^+$ (for A2) or $Li(H_2O)_4^+$ (for A3) (Tables 2 and 5). b. The difference between the two curves in (a) (dashed line) is compared with the difference between the experimental $D(r)-4\pi r^2\rho_0$ functions for the A2 and A3 solutions (solid line). c. The difference between the peak shapes obtained if water is not assumed to be coordinated to zinc in the $ZnBr_3^-$ and the $ZnBr_2$ complexes.

a planar triangular complex (120°). The experimental data do not allow separate refinements for the $ZnBr_3^-$ and the $ZnBr_2$ complexes, and in the C solutions, in which the relative proportions of lower complexes is the largest, the number of Zn–Br interactions is too small for a least-squares refinement to give precise values.

In the short-distance region of the $D(r)$ functions the major contributions come from intramolecular interactions. Differences between the $D(r)$ curves for the concentrated A solutions, which all have the same total bromide concentration, will then reflect primarily differences between the complexes. Intermolecular interactions will not contribute at short distances and may be expected not to differ much at longer distances, apart from a continuous increase when Li^+ is replaced by Zn^{2+}. The largest differences in concentrations occur between A3 and A2 for $ZnBr_3^-$ and between A2 and A1 for $ZnBr_2$ (Table 3) and the corresponding difference curves should be best suited for giving information on their structures. In Figs. 5 and 6 the difference curves A2–A3 and A1–A2 are compared with differences between calculated peak shapes for some conceivable models.

The pyramidal structure for $ZnBr_3^-$ with a Br–Zn–Br angle of about 114° follows from the least-squares results (Tables 2 and 4). This is the same as the value found for the discrete units $ZnBr_3H_2O^-$ (average Br–Zn–Br angle ~113°) in crystals of α- and β-$KZnBr_3 \cdot 2H_2O$,[25,26] and it seems likely that a water molecule is coordinated to $ZnBr_3^-$ also in solution. Two models, $ZnBr_3^-$ and $ZnBr_3H_2O^-$, are used for the comparison in Fig. 5.

For $ZnBr_2$ a bent structure with a Br–Zn–Br angle about 115° (Table 4) would seem likely, but the number of Br–Br interactions in $ZnBr_2$ is too small to make a significant contribution to the scattering data. In an assumed linear structure with Zn–Br bond lengths of 2.38 Å (Table 4) water molecules would not be able to approach Zn^{2+} to within the expected Zn–H_2O bonding distance of about 2.1 Å, as that would lead to too short Br–H_2O distances (3.17 Å). A complex of this type would, therefore, be very weakly solvated. If Zn^{2+} in $ZnBr_2$ were octahedrally

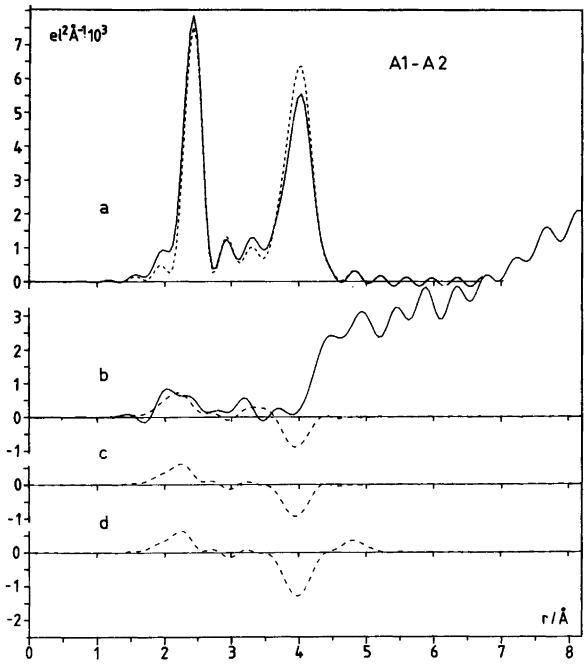

Fig. 6. a. Peak shapes calculated for the complexes in the A1 (solid line) and the A2 (dashed line) solution. b. The difference between the peak shapes in (a) (dashed line) compared with the difference between the experimental $D(r)-4\pi r^2\rho_o$ functions (solid line). c. The difference between the peak shapes obtained if no water is assumed to be coordinated to Zn in the bent $ZnBr_2$ structure. d. The corresponding difference assuming a linear, nonhydrated $ZnBr_2$ complex.

coordinated by $2Br^-$ and $4H_2O$ we would expect a lengthening of the Zn–Br bonds to about 2.7 Å, analogous to that found for Zn–Cl bonds in the octahedral $ZnCl_2(H_2O)_4$ complexes in crystals of $ZnCl_2 \cdot 1\frac{1}{3}H_2O$[27] or in the octahedral $Zn(N_2H_4)_4Cl_2$ in crystals of $Zn(N_2H_4)_2Cl_2$.[28] Here, the Zn–Cl bonds are about 0.3 Å longer than the tetrahedral bonds. This is not, however, consistent with the spectroscopic data and, therefore, the models for the $ZnBr_2$ complex used for the comparison in Fig. 5 have been limited to a linear non-hydrated $ZnBr_2$ unit with Zn–Br bond lengths of 2.38 Å, a bent non-hydrated $ZnBr_2$, and an approximately tetrahedral $ZnBr_2(H_2O)_2$.

Compared to the calculated peak shapes (Figs. 5 and 6), the differences between the models are small. In both A1 and A2 each Br forms one Zn–Br bond and with the data normalized to one Br atom the Zn–Br peaks will be equal in size. In the A1–A2 difference curve (Fig. 6), the peak at about 2 Å results from Zn–H_2O interactions, but even if water is bonded to Zn in the lower zinc bromide complexes, the major contributions to this peak will come from the hydrated Zn^{2+} ions (Table 3). In the A2 and A3 solutions the amount of free Zn^{2+} is small (Table 3) and the 2 Å peak does not appear separately in the A2–A3 difference curve (Fig. 5). Here, the peak at 2.4 Å results from the smaller number of Zn–Br bonds per Br atom in the A3 solution.

Beyond about 4 Å intermolecular interactions begin to appear and the difference curves will increase. These interactions overlap the intramolecular Br–Br interactions and the difference curves will not be very sensitive towards different assumptions about the number of Br–Br interactions in the lower complexes.

A presence of water molecules in the $ZnBr_3^-$ and the $ZnBr_2$ complexes can be determined only by identifying intramolecular Br–H_2O interactions, which should appear at about 3.5 Å. The comparison in Figs. 5 and 6 with curves calculated for the different models shows a slightly

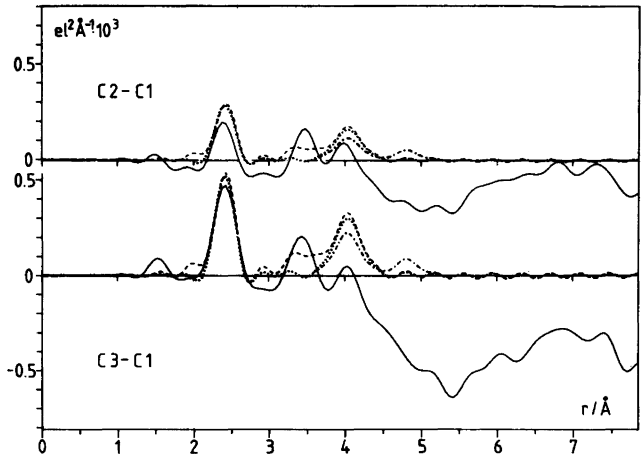

Fig. 7. Differences between experimental $D(r)-4\pi r^2\rho_o$ functions for the C solutions (solid lines), after subtracting calculated intramolecular contributions from ClO_4^-, $ZnBr_4^{2-}$ and $Zn(H_2O)_6^{2+}$, compared with differences between calculated peak shapes with (dashed lines) or without (dotted lines) water coordinated to Zn in the $ZnBr_3^-$ and the $ZnBr_2$ complexes. The dashed-dotted line is obtained by a linear, non-hydrated $ZnBr_2$ structure.

better agreement for $ZnBr_3H_2O^-$ and $ZnBr_2(H_2O)_2$ than for $ZnBr_3^-$ and $ZnBr_2$. The differences are small, however, and may well be affected by possible differences in intermolecular Br–H_2O interactions. Difference curves calculated for the C series of solutions (Table 1), where the lower complexes are relatively more dominant, lead to similar results (Fig. 7). The Zn–Br and the Br–Br peaks, obtained after removing calculated intramolecular contributions from ClO_4^-, $ZnBr_4^{2-}$ and $Zn(H_2O)_6^{2+}$, are consistent with values expected for the $ZnBr_3^-$ and $ZnBr_2$ complexes (Table 4). Inclusion of water molecules in the models has a marked influence on the calculated peak shapes and the resulting intramolecular Br–H_2O peak at 3.5 Å has a correspondence in a peak in the experimental difference curves (Fig. 7). However, intermolecular Br–H_2O interactions can be expected to contribute in the same region, which makes an interpretation ambiguous. A linear rather than a bent $ZnBr_2$ structure is not supported by the data (Fig. 7) but the expected effects of the structural difference are again small and close to the noise level of the difference curves. We conclude that the diffraction data do not lead to an unambiguous interpretation but seem to give some support for the occurrence of $ZnBr_3H_2O^-$ and $ZnBr_2(H_2O)_2$ with approximately tetrahedral structures.

The peak at 2.8 Å in the A2–A3 difference curve is probably due to water–water interactions and can be reproduced (Fig. 5) by assuming the Li^+ ion to be coordinated tetrahedrally by four H_2O in A3 but octahedrally by six H_2O in A2 (Table 5). For each solution, this corresponds approximately to the total number of available water molecules (Table 3). In A1, which contains no Li^+, part of the water will be free (Table 3) and not bonded to Zn, and in the theoretical difference curve (Fig. 6) H_2O–H_2O interactions at 2.8 Å have been included (Table 5).

When treating the data for the more dilute solutions "B" in the same way, similar results are obtained. The differences between the experimental $D(r)$ functions are well reproduced by the theoretical curves obtained with the parameters in Tables 3, 4 and 5. The relative contributions from the intramolecular interactions are smaller here, and peaks in the difference curves are even less pronounced than for the A solutions. For the same Br–Zn ratio, the relative concentrations of the lower complexes are higher in the more dilute B series than in the A series of solutions (Tables 2 and 3), reflecting the stronger competition from water molecules for positions within the coordination sphere of the Zn^{2+} ion in these solutions.

Table 5. Parameter values used for the calculations of theoretical curves.

	Complexes						
	$ZnBr_4^{2-}$	$ZnBr_3^-$	$ZnBr_2$	$Zn(H_2O)_6$	ClO_4^-	$Li(H_2O)_4^+$	$Li(H_2O)_6^+$
d_{M-L} Å	2.408	2.386	2.386	2.10	1.420	1.91	2.02
d_{L-L} Å	3.93	4.00	4.01	2.97	2.32	3.12	2.86
b_{M-L} Å^2	0.003	0.003	0.003	0.012	0.0008	0.002	0.004
b_{L-L} Å^2	0.015	0.015	0.015	0.02	0.0016	0.004	0.01
R Å	4.5	4.0	4.0	4.0	3.6	4.0	4.0
B Å^2	0.17	0.17	0.17	0.17	0.08	0.17	0.17

Intermolecular interactions (frequencies referred to the first atom in the pair).

		A1	A2	A3	B1	B2	B3	C1	C2	C3
	d	–			2.85	2.85	2.85	2.90	2.87	2.85
H_2O-H_2O	b	–			0.03	0.02	0.02	0.01	0.005	0.012
	n	–			1.24	0.74	0.34	1.62	1.01	1.26
	d	3.85	3.50	3.50	3.45	3.40	3.40		3.50	3.45
Br—H_2O	b	0.07	0.05	0.07	0.03	0.02	0.02		0.15	0.15
	n	2.9	3.0	6.0	5.0	5.0	4.8		8.0	6.0
	d	4.18	4.15	4.20	4.15	4.15	4.02			
Br—Br	b	0.05	0.05	0.05	0.04	0.05	0.05			
	n	0.83	0.90	0.80	0.60	0.60	0.60			
	d							3.95	3.95	4.10
Zn—H_2O	b							0.15	0.15	0.20
	n							14.0	12.0	12.0
	d							3.70	3.50	3.45
Cl—H_2O	b							0.20	0.15	0.15
	n							7.0	9.0	6.0

Spectroscopic data. In principle, the structures of species in solution should be distinguishable on the basis of IR and Raman spectra. For solution A3, the observations (Fig. 8) are in agreement with the predictions for a regular tetrahedral $ZnBr_4^{2-}$ ion, and there is no indication of any other zinc complex being present. The T_2 stretching vibration is observed at 207 cm^{-1} in the IR spectrum (Fig. 8).

All other zinc bromide solutions studied contain a number of zinc complexes. It is clear from the Raman spectra obtained here and from the work of Macklin and Plane[15] that Zn–O stretching vibrations do not provide a useful diagnostic tool because only for $Zn(H_2O)_6^{2+}$ has such a vibration been observed. It is presumed that such bonds are too polar in character to generate sufficient Raman intensity. IR spectra are not helpful either in identifying Zn–O stretching vibrations because the appropriate frequency range is the same as that in which very intense and broad librational bands from free and complexed water molecules occur.[29] Below the range of Zn–Br stretching vibrations, the Raman spectra are comparatively simple and we must conclude that the only deformation modes which contribute observable intensity involve Br–Zn–Br angles.

The symmetric stretching vibrations of $ZnBr_4^{2-}$, $ZnBr_3^-$ and $ZnBr_2$ are sufficiently well resolved in the Raman spectra to show the co-occurrence of these complexes, and curve resolution of these features has been used above in the estimation of concentrations of the species, in conjunction with the X-ray studies. However, the composite spectra do not provide clear structural evidence. The Br–Zn–Br deformation region below 100 cm^{-1} consists of overlapping contributions from different species and the bands are not resolved even after subtraction of the rising solvent profile.

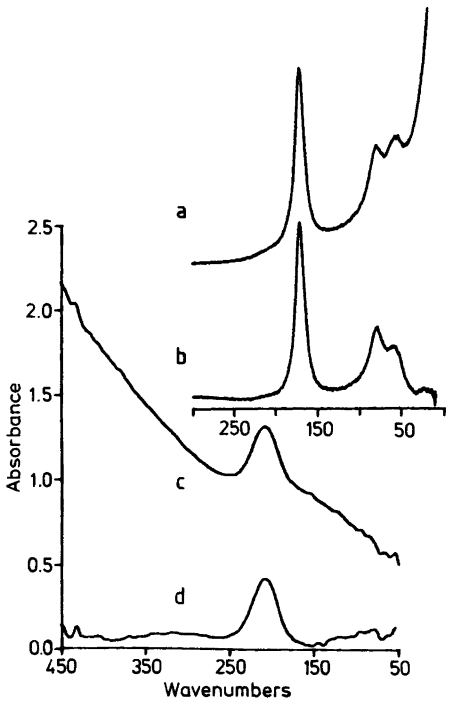

Fig. 8. Raman spectrum of solution A3 as measured (a), after subtraction of water spectrum (b), and infrared spectrum, as measured (c), after subtraction of water and "$Li(H_2O)_4Br$" (d).

(Spectra tend to show a band below 25 cm^{-1} which is not considered to be due to the ZnBr complex but to arise from alteration in the steep water profile at very low wave numbers between water and the solutions). To clarify this region below 300 cm^{-1}, we have used spectral subtraction methods. Because A3 contains only $ZnBr_4^{2-}$, its spectrum was used interactively to null the contribution of this species to A2 and A1. This leaves spectra ("A2" and "A1") which essentially contain $ZnBr_2$ and $ZnBr_3^-$ species in different ratios. Interactive interplay of these residual spectra should enable the spectrum of $ZnBr_3^-$ to be isolated from subtraction of "A1" from "A2", and that of $ZnBr_2$ by the reverse subtraction. This is illustrated in Fig. 9. In this instance the method only serves to identify intense features with certainty (104 and 69 cm^{-1} for $ZnBr_3^-$ and 205 for $ZnBr_2$); ν_1 of $ZnBr_4^{2-}$ does not exactly coincide in position and band shape for the three solutions and this leads to imperfect subtraction.

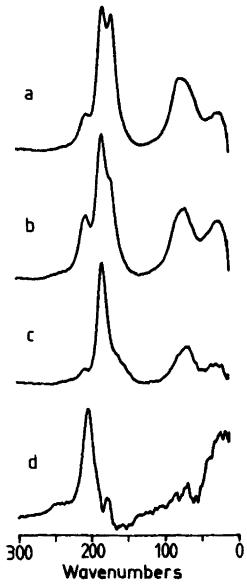

Fig. 9. Raman spectrum (after water subtraction) of solution A2 (a), solution A1 (b), and results of spectral interplay to isolate features due to $ZnBr_3^-$ (c),and $ZnBr_2$ (d).

The numbers of bands definitely identified are no greater than required for the highest symmetry possibilities.

We have attempted to use a similar technique with IR spectra. In this case, the Zn–Br stretching bands are not resolved and so we cannot use visual methods to monitor the separation of individual components. However, because cell thicknesses are known and intensities absolutely related to concentration, we have used the results of Table 6 for subtraction of the $ZnBr_4^{2-}$ component from solutions A1 and A2 and attempted to isolate the contributions from $ZnBr_3^-$ and $ZnBr_2$ by further rounds of subtraction in the same way. The result for $ZnBr_3^-$ does show two features in the Zn–Br stretching region (Fig. 10), an intense band at 229 cm^{-1} and a weak feature at 186 cm^{-1}, coincident with the intense Raman band. This observation supports a pyramidally distorted structure rather than a planar one, and agrees with the report by Waters *et al.*[30] for $ZnBr_3^-$ in tri-n-butyl phosphate solution. Because the 186 cm^{-1} band is a little more intense than the noise level, we have also examined the spectrum of B1 in a similar way and have found that it is reproducible. Our attempts at isolating the spec-

Table 6. Relative intensities from curve analysis of Raman spectra in the Zn—Br stretching region and relative proportions of $ZnBr_n^{(2-n)+}$ complexes on the basis of published relative intensities.[15]

	Relative integrated intensities				Relative proportions			
cm^{-1}	171	184	207	237	$ZnBr_4^{2-}$	$ZnBr_3^-$	$ZnBr_2$	$ZnBr^+$
$\Delta\nu_{1/2}$ cm^{-1}	14.0	14.6	15.2	~15[a]				
A1	26.1	52.3	21.4		21.5	42.0	36.5	
A2	42.1	48.4	9.4		38.8	43.3	17.9	
A3	100				100			
B1	36.9	50.7	12.2		33.1	44.2	22.7	
B2	48.7	44.3	6.9		45.2	41.6	13.2	
B3	60.9	36.0	3.0		59.7	34.2	6.1	
C2	13.2	52.8	30.5	3.4	9.3	36.0	44.2	10.6
C3	21.7	51.3	24.8	1.9	16.6	38.0	39.1	6.4

[a] Rough value since this feature is never a major component.

trum of $ZnBr_2$ have not been successful as no features result in the Zn–Br stretching region of intensity greater than the general noise level of the resulting spectrum.

On the presumption that complexing by methanol or water would yield similar species, we have made a limited study of vibrational spectra of zinc bromide species in undried methanol. Again mixtures of complexes are observed but with this solvent the Zn–Br stretching bands are sharper in the IR (*e.g.* Fig. 11). This allows interactive subtraction methods to be used visually to isolate contributions from individual species (Fig. 12). The Raman spectrum of a 2 M $ZnBr_2$ solution has a strong polarised band due to $ZnBr_2$ and a weaker one due to $ZnBr_3^-$. At a composition of 2 M $Li_{1.4}ZnBr_{3.4}$ the predominant species is $ZnBr_3^-$, whilst at 1.6 M $Li_{3.5}ZnBr_{5.5}$, $ZnBr_4^{2-}$ appears to be the sole zinc complex present. Use of these and the corresponding IR spectra interactively, after subtraction of the solvent spectrum and contribution from the solvated lithium ion, yields spectra for the individual contributions (Fig. 12). The spectra of $ZnBr_4^{2-}$ closely resemble those observed from aqueous solution. The Raman spectrum of $ZnBr_3^-$ has a weak broad band about 230 cm^{-1}, an intense polarised band at 183 cm^{-1} and a broad deformation band which

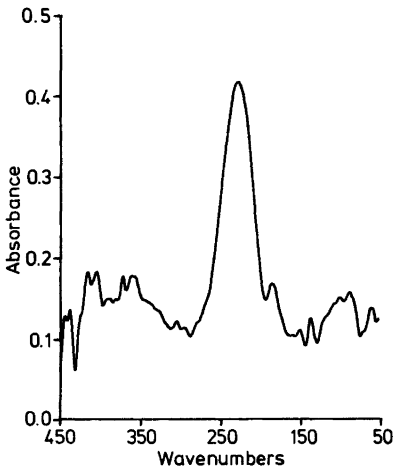

Fig. 10. Infrared features due to "$ZnBr_3$" isolated by spectral subtraction.

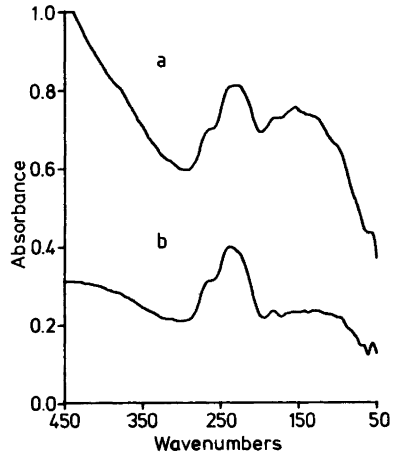

Fig. 11. Infrared spectrum of 2 M $Li_{0.7}ZnBr_{2.7}$ in methanol as measured (a), after spectral subtraction of MeOH and "$Li(MeOH)_4Br$" (b).

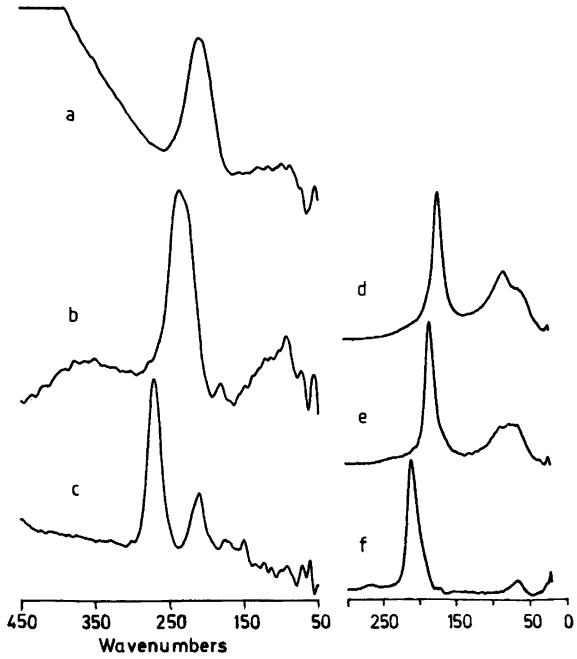

Fig. 12. Infrared features due to $ZnBr_4^{2-}$ (a), $ZnBr_3^-$ (b) and $ZnBr_2$ (c) in methanol, isolated by spectral subtraction. Raman features due to $ZnBr_4^{2-}$ (d), $ZnBr_3^-$ (e) and $ZnBr_2$ (f) in methanol, isolated by spectral subtraction.

depolarisation measurements show to consist of two components, a polarised contribution about 87 cm^{-1} and a depolarised band at 72 cm^{-1}. The IR spectrum shows two Zn–Br stretching bands 238 and 183 cm^{-1} (*cf.* Fig. 12 and 10). These results are fully consistent with a pyramidal structure for the species in methanol and the similarity of frequencies to those found in aqueous solution lends support to similarity of structures in the two solvents.

For $ZnBr_2$, the spectra are much more informative than those derived from aqueous studies. There is a weak, high-frequency Zn–Br stretching band at 269 cm^{-1} coincident with a strong IR band. The intense polarised Raman band at 210 cm^{-1} also has a counterpart in the IR spectrum; these findings are comparable to those of Waters *et al.*[30] for $ZnBr_2$ in tri-n-butyl phosphate. The Raman spectrum also shows a single deformation band at 68 cm^{-1}. Thus, these observations are fully in agreement with a bent $ZnBr_2$ structure. The vibrational frequencies clearly established for the particular species are summarised in Table 7.

Table 7. Vibrational spectra of zinc bromide complexes in aqueous and methanol solutions.

Water IR	Raman		MeOH IR	Raman
$ZnBr_4^{2-}$		T_d		
207 s	~205 sh	$\nu_3(T_2)$	210 vs	210 w
	171 vs p	$\nu_1(A_1)$		170 vs p
	80 m dp	$\nu_4(T_2)$		81 m dp
	60 m dp	$\nu_2(E)$		62 m dp
$ZnBr_3^-$		C_{3v}		
229 vs		$\nu_3(E)$	238 vs	238 vw
185 w	184 vs p	$\nu_1(A_1)$	183 w	183 vs p
	79 sh	$\nu_2(A_1)$		87 m p
	69 m	$\nu_4(E)$		72 m dp
$ZnBr_2$		C_{2v}		
	245 br	$\nu_3(B_1)$	268 s	269 w
	205 vs p	$\nu_1(A_1)$	211 m	210 vs p
		$\nu_2(A_1)$		68 m

These structural conclusions agree with those of Macklin and Plane[15] for aqueous solutions.

These authors, however, relied on curve analysis of broad composite bands in the deformation region to identify weak features on the edge of the strong solvent profile. From our aqueous studies, there is certainly no deformation feature for $ZnBr_3^-$ at 49 cm^{-1}; if a second deformation band is present, it is on the high frequency side of 69 cm^{-1}, *i.e.* similar to the observation from MeOH solution.

CONCLUSION

The combined information from X-ray diffraction, Raman and IR measurements seems to give strong evidence for a pyramidal structure for $ZnBr_3^-$ and a bent structure for $ZnBr_2$ in aqueous solution. The highest complex formed, $ZnBr_4^{2-}$, is tetrahedral, as is well known from previous investigations. In the solutions investigated, the $ZnBr^+$ complex is only at best a very minor component; consequently no structural details could be obtained. It seems likely that water molecules are coordinated to zinc in the $ZnBr_3^-$ and the $ZnBr_2$ complexes, completing approximately tetrahedral structures, but the methods used are not capable of providing clear confirmation; $Zn-H_2O$ bonds within the complexes give too weak contributions to the spectra to be observed and in the diffraction data, the expected intramolecular $Br-H_2O$ interactions give only small contributions which are masked by contributions from intermolecular $Br-H_2O$ interactions occurring at approximately the same distance.

Acknowledgements. This work has been supported by the Swedish Natural Science Research Council (NFR). We thank Mr Ernst Hansen for skillful technical assistance.

REFERENCES

1. Sillén, L. G. and Martell, A. E. *Spec. Period. Publ.: Stability Constants 17* (1964); *Suppl. 25* (1970); Högfeldt, E. *Stability Constants of Metal Ion Complexes Part A: Inorganic Ligands,* Pergamon, Oxford 1982.
2. Ahrland, S., Kullberg, L. and Portanova, R. *Acta Chem. Scand. A 32* (1978) 251.
3. Debot, F. *Physica 21* (1955) 605.
4. Kruh, R. F. and Standley, C. L. *Inorg. Chem. 1* (1962) 941.
5. Wertz, D. L. and Bell, J. R. *J. Inorg. Nucl. Chem. 35* (1973) 137, 861.
6. Kálmán, E., Serke, I., Pálinkás, G., Johansson, G., Kabiscj, G., Maeda, M. and Ohtaki, H. *Z. Naturforsch. Teil A 38* (1983) 225.
7. Wertz, D. L., Lawrence, R. M. and Kruh, R. F. *J. Chem. Phys. 43* (1965) 2163.
8. Lagarde, P., Fontaine, A., Raoux, D., Sadoc, A. and Migliardo, P. *J. Chem. Phys. 72* (1980) 3061.
9. Delwaulle, M. L. *Compt. Rend. 240* (1955) 2132.
10. Yellin, W. and Plane, R. A. *J. Am. Chem. Soc. 83* (1961) 2448.
11. Morris, D. F. C., Short, E. L. and Waters, D. N. *J. Inorg. Nucl. Chem. 25* (1963) 975.
12. Irish, D. E., McCarroll, B. and Young, T. F. *J. Chem. Phys. 39* (1963) 3436.
13. Quicksall, C. O. and Spiro, T. G. *Inorg. Chem. 5* (1966) 2232.
14. Gilbert, B. *Bull. Soc. Chim. Belg. 76* (1967) 493.
15. Macklin, J. W. and Plane, R. A. *Inorg. Chem. 9* (1970) 821.
16. Beer, J., Crow, D. R., Grzeskowiak, R. and Turner, I. D. M. *Inorg. Nucl. Chem. Lett. 9* (1973) 35.
17. Johansson, G. *Acta Chem. Scand. 20* (1966) 553.
18. Johansson, G. and Sandström, M. *Chem. Scr. 4* (1973) 195.
19. Norman, N. *Acta Cryst. 10* (1957) 370.
20. Krogh-Moe, J. *Acta Cryst. 9* (1956) 951.
21. *International Tables for X-Ray Crystallography,* Kynoch Press, Birmingham 1974, Vol. 4.
22. Cromer, D. T. *J. Chem. Phys. 50* (1969) 4857.
23. Cromer, D. T. and Mann, J. B. *J. Chem. Phys. 47* (1967) 1892.
24. Carr, C. and Goggin, P. L. *J. Mol. Struct. 79* (1982) 261.
25. Follner, H. and Brehler, B. *Acta Crystallogr. B 24* (1968) 1339.
26. Holinski, R. and Brehler, B. *Acta Crystallogr. B 26* (1970) 1915.
27. Follner, H. and Brehler, B. *Acta Crystallogr. B 26* (1970) 1679.
28. Ferrari, A., Braibanti, A. and Bigliardi, G. *Acta Crystallogr. 16* (1963) 498.
29. Draegert, D. A., Stone, N. W. B., Cevnette, B. and Williams, D. *J. Opt. Soc. Am. 56* (1966) 64.
30. Waters, D. N., Short, E. L., Tharwat, M. and Morris, D. F. C. *J. Mol. Struct. 17* (1973) 389.

Received March 29, 1984.